J Mater Sci: Mater Med (2008) 19:753–759
DOI 10.1007/s10856-007-3085-7

Bone resembling apatite by amorphous-to-crystalline transition driven self-organisation

Yassen Pekounov · Ognyan E. Petrov

Received: 7 May 2006 / Accepted: 1 May 2007 / Published online: 10 July 2007

Abstract Calcium apatite is the main inorganic constituent of mammalian hard tissues such as bones and teeth. Its formation in vivo is likely to be preceded by a transient amorphous phase. If so, the amorphous-to-crystalline transition would have some crucial role in the biomineralisation process. To investigate this possibility, a two-step biomimetic experiment was designed. First, a stable amorphous calcium apatite precursor was synthesized in simulated body fluid (SBF) and was then transformed into a low crystalline apatite. X-ray diffraction (XRD), Fourier transform infrared (FTIR) spectroscopy, vacuum FTIR, inductively coupled plasma-atomic emission spectrometry (ICP-AES), scanning electron microscopy (SEM) and N_2 adsorption measurements were used to characterise both the precursor and the apatite. The latter exhibits numerous bone-like features including lack of OH, nanometer size, low crystallinity, etc. An amorphous-to-crystalline transition driven self-organisation is observed. The amorphous precursor seems to be the essential step for the creation of bone resembling apatite.

Introduction

Calcium apatite is the main mineral constituent of bone. Therefore, it attracts much research interest since it could be used for bone tissue repair and as a biocompatible coating on artificial implants [1]. Nevertheless, the synthesis of a completely bioanalogous calcium apatite is still challenging.

In vivo biomineralisation process is likely to be a two step one. Initially, an amorphous phase is formed, which subsequently transforms into a crystalline solid [2, 3]. Currently, this possibility is supported by numerous biomimetic model studies. An amorphous calcium apatite precursor (ACAP) is usually found in experiments with synthetic physiological solutions such as Kokubo's simulated body fluid (SBF) [4–6]. ACAP is detected in more complicated model systems containing biopolymers such as gelatin, phosvitin, and remarkably dentin matrix protein 1 [7–10]. It was demonstrated that an amorphous calcium phosphate phase plays a key intermediate role in the initial matrix vesicles induced mineralisation [11, 12]. Moreover, a general relationship between the amorphous precursor and calcium apatite was established [13], namely that both phases are constituted by the same building block—the so-called Posner's cluster ($Ca_9(PO_4)_6$). Further on, it was revealed that the Posner's cluster with the expected size and chemical formula exists in various kinds of SBFs [14, 15].

Natural bone calcium apatite is poorly crystalline and calcium deficient carbonate apatite with several ionic substitutions [1]. Probably, in bone apatite there is no detectable amount of hydroxyl groups [16, 17]. Other features are the nanometer size and the high surface area, i.e., 100–200 m^2/g [18]. Thus, a bone resembling apatite should be at least nanometric, low crystalline and hydroxyl-free with a surface area and chemical composition similar to these of natural bones.

Biomimetics is a suitable strategy for the engineering of bioanalogous materials with desired properties. Therefore, in this study we investigate the possibility to use an

Ya. Pekounov (✉)
Institute of General and Inorganic Chemistry,
Bulgarian Academy of Sciences, Sofia 1113, Bulgaria
e-mails: ya.pekounov@gmail.com; pekounov@svr.igic.bas.bg

O. E. Petrov
Central Laboratory of Mineralogy and Crystallography,
Bulgarian Academy of Sciences, Sofia 1113, Bulgaria

amorphous calcium apatite precursor in order to produce bone-similar apatite.

Materials and methods

Preparation of materials

Reagent and analytical grade chemicals (Fluka or Merck) and distilled deionised (dd) water were used. In order to avoid Si contamination all the experiments were performed in polypropylene or Teflon vessels [19].

Amorphous calcium apatite precursor (ACAP) was synthesized in simulated body fluid [5]. Two distinct calcium and phosphorus solutions were prepared by dissolving the appropriate amount of salts (Table 1). Ca/P molar ratio was kept to 2.5 while Ca and P concentrations were 40 times greater than the concentrations of human plasma respectively SBF (Table 2). To compensate the so introduced high amount of sodium and chlorine ions, no NaCl was added. In order to reduce the transformation rate of ACAP, cold dd water (~4 °C) was used [20]. The pH of Ca solution was adjusted to 3 with 1 M HCl to avoid $CaCO_3$ precipitation [5]. About 15 mL 5 M NaOH were added to P solution. The stock solutions were rapidly mixed and vigorously stirred until pH was stabilized. The latter process took less than a minute and the pH value was slightly under 8. Thus obtained gel-like precipitate was filtered, triply washed with cold dd water, not completely dried at 60 °C and finally desiccated over silica gel at room temperature. Typically, the filtration procedure prolonged more than 30 min. The material remains amorphous for at least 6 months. It should be noted that temperature as low as 60 °C is enough to induce the crystallisation of the dry ACAP and that the higher the precipitation the greater the transformation rate is [21].

ACAP was transformed into a more or less crystalline calcium apatite (CAp) via maturation in SBF at 37 °C in closed Teflon vessel. SBF was prepared as described elsewhere [5]. Typically, 0.2 g ACAP was immersed in 100 mL SBF for times ranging from 5 min up to 48 h. After desired time periods, the samples were filtered, triply washed with dd water and dried in air. The features of the final apatites thus obtained were not affected by the solid to liquid ratio in a wide range.

Table 2 Ion concentrations of ACAP solution, SBF [5], and human plasma [14]

Ion	ACAP (mM)	SBF (mM)	Human plasma (mM)
Na^+	183[a]	142.0	142.0
Cl^-	208	125.0	103.0
HCO_3^-	27.0	27.0	27.0
K^+	5.0	5.0	5.0
Mg^{2+}	1.5	1.5	1.5
Ca^{2+}	100	2.5	2.5
HPO_4^{2-}	40	1	1
SO_4^{2-}	0.5	0.5	0.5

[a] NaOH supplement was considered in the calculation

Methods

Powder XRD was performed to control the crystallisation status of the apatite structure using a DRON-3 M diffractometer (Fe-filtered CoK_α radiation) and applying step-scanning approach. The samples were scanned from 8° to 60° (2θ) using steps of 0.02° (2θ) and counting time of 3 s per step. The WinFit V1.2 software helped to determine the peak positions and to evaluate the crystallite size with time [22].

FTIR spectroscopy was used to investigate the crystallinity as well as to evaluate the carbonate substitution. The IR spectra were recorded on Nicolet Avatar 360 spectrometer at a spectral resolution of 2 cm^{-1} and accumulation of 64 scans using KBr technique. The number and the exact positions of the overlapping bands in the υ_3 carbonate stretching region about 1,600–1,300 cm^{-1} were determined using Fourier self-deconvolution (FSD) procedure by means of Omnic™ software (Thermo Electron Corp.). The smoothed spectra were automatically deconvoluted using Happ-Genzel apodization and were then corrected to contain no more than six peaks in the resolved region. The carbonate content measurements were accomplished with Omnic™ software as well. Since the integrated intensity is proportional to the concentration, the integral peak areas of the υ_3 carbonate stretching region were calculated for the region between 1,565 cm^{-1} and 1,365 cm^{-1} with an automatic base-line correction. $CaCO_3$ was used as a standard.

Vacuum FTIR was performed to determine the hydroxyl content. Self-supporting pellets (ca. 10–20 mg cm^{-2}) were

Table 1 Chemical composition of ACAP solutions

Reagent	Ca solution		Reagent	P solution	
	Purity (%)	Amount (g/l)		Purity (%)	Amount (g/l)
$CaCl_2{\cdot}2H_2O$	99	14.80	Na_2HPO_4	99.5	5.70
KCl	99.5	0.375	$NaHCO_3$	99.5	2.268
$MgCl_2{\cdot}6H_2O$	99	0.305	Na_2SO_4	99	0.074

prepared from pure sample powder and treated directly in the purpose-made IR cell equipped with a heat treatment device. The cell was connected to a vacuum-adsorption apparatus with a residual pressure below 10^{-3} Pa. The samples were heated to 400 °C in vacuum to remove water content [23, 24], which enables the registration of hydroxyl groups in apatite structure [17]. The spectra were recorded as described. It should be noted that the vacuum cuvette is equipped with CaF_2 glasses which explains the different cut-off values between the two FTIR protocols used in this study since CaF_2 absorbs under about 1,000 cm^{-1}.

ICP-AES was used to determine the elemental composition and to calculate the Ca/P molar ratio. The samples were dissolved in HNO_3 and the analyses were performed with a Jobin Yvon (JY ULTIMA 2) apparatus equipped with a 1 m Cserny-Turner monochromator and a 40,68 MHz ICP. In certain cases the Ca/P molar ratio was verified with chemical analysis.

Particle size distribution and morphology were investigated using JEOL 5510 scanning electron microscope. The samples were gold sputtered prior to examination in argon atmosphere by means of JEOL JFC-1200 device.

The specific surface area of the samples was measured by N_2 BET method using an apparatus described elsewhere [25].

Results

In this section four samples are discussed—the amorphous calcium apatite precursor (ACAP) and three crystalline ones denoted as SBF 2 h, SBF 24 h and SBF 48 h according to their maturation time in SBF.

Figure 1 shows the XRD spectra of these samples. ACAP exhibits typical spectrum of noncrystalline material where only amorphous halo is observed. SBF 2 h, SBF 24 h and SBF 48 h show some degree of crystallinity, which, as expected, increases with soaking in SBF. However, the apatite peaks in the pattern are not well resolved due to the nanometer size of thus obtained material [23, 24]. The crystallite size determined using peaks with *hkl* indices 002 and 211 slightly increases from about 7.4 nm and 1.5 nm, respectively, (SBF 2 h) to 9.2 nm and 2.5 nm (SBF 24 h) [26]. There is no further increase in crystallite size after 24 h maturation period suggesting some SBF-driven inhibitory effect on the crystal growth.

The crystallisation process was also followed by FTIR (Fig. 2). For this purpose the increase of the characteristic splitting in the υ_4 phosphate vibrational region about 530–630 cm^{-1} was monitored [27, 28]. The smooth spectrum of ACAP in this region is an evidence for an amorphous state while the sustained splitting occurring with its soaking in SBF confirms the increasing crystallinity of thus obtained

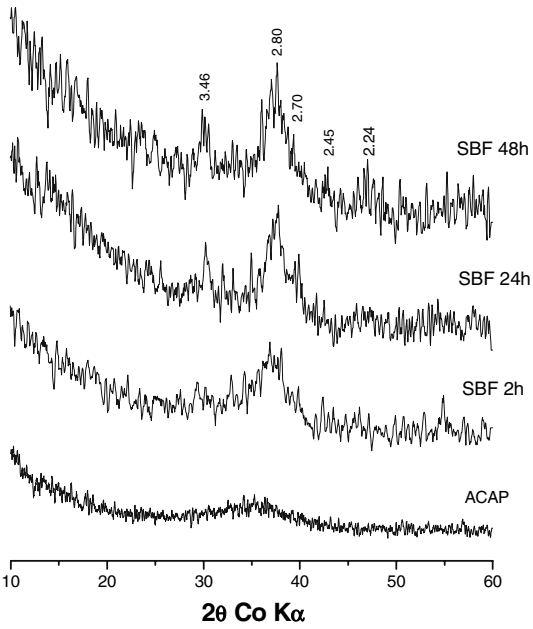

Fig. 1 Powder X-ray diffraction patterns of the samples

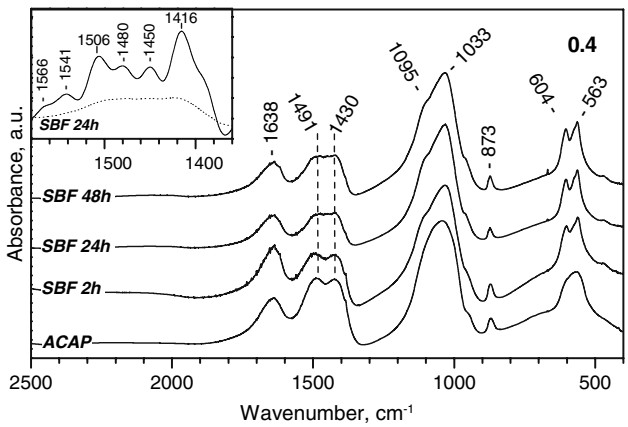

Fig. 2 FTIR spectra of the specimens. The inset displays the Fourier self-deconvoluted spectrum (*solid line*) and raw data superimposed (*dotted line*) of the carbonate asymmetric stretching vibration region of SBF 24 h sample. The resolved spectrum shows only the existence of type A–B carbonate apatite bands and neither the peaks intensities nor their areas are in scale

apatite. Notably, the crystallisation status in the initial period of transformation (less than 2 h) can be followed only by IR spectroscopy, but not by XRD analysis. The carbonate content in ACAP is demonstrated with the peaks at 1,491, 1,430, and 873 cm^{-1} [29]. The latter is about 7.5 wt% for ACAP and slightly decreases with increase of crystallinity [23]. With maturation the υ_3 carbonate vibrational region about 1,450 cm^{-1} becomes unresolved and SBF 24 h and SBF 48 h apatites exhibit an unusual broadening. As known the carbonate ions can substitute both for hydroxyl ions (that is A-type substitution) and for

phosphate ions (B-type substitution). It is possible that the observed broadening is due to A–B type substituted apatite. If so, a characteristic IR signature should be present containing three doublet bands that correspond to the three structural locations, which the carbonate ions can occupy in the apatite lattice, denoted as A1 position (bands at 1,540 and 1,451 cm^{-1}), A2 position (bands at 1,571 and 1,506 cm^{-1}) and B position (bands at 1,475 and 1,416 cm^{-1}) [30, 31]. However, the exact positions of these bands can vary among different samples, but not greatly [30, 31]. The inset of Fig. 2 shows the Fourier self-deconvoluted spectrum of the SBF 24 h sample confirming the presence of characteristic IR signature of type A–B carbonate apatite. It should be noted that SBF 48 h specimen exhibits as well a characteristic IR signature of type A–B carbonate apatite while ACAP and SBF 2 h sample do not (data not shown).

Further, we used vacuum FTIR to check whether there are hydroxyl groups as the lack of OH is a possible significant bone feature [16]. Figure 3a shows the IR spectrum of SBF 48 h at 25 °C. The broad absorption peak at 3,400 cm^{-1} and this at 1,637 cm^{-1}, which disable the IR observation of the apatitic OH groups [17], are typical for water associated with CAp [33]. Figure 3b exhibits the spectrum of a carbonate apatite after removing the water as described earlier. The peaks at 3,400 and 1,637 cm^{-1} vanished while a new peak ascribed to apatite OH stretching mode appeared at 3,569 cm^{-1} [33]. The spectrum of water depleted SBF 48 h sample is shown on Fig. 3c. Apparently, there is no detectable amount of hydroxyl ions. The band at 1,233 cm^{-1} (Fig. 3a) is ascribed to P–OH in-plane deformation [34] due to adsorbed water. This peak cannot be detected in KBr pellets (Fig. 2) but only in pure sample powder self-supporting pellets due to their very high signal intensity and is directly related to the water content of the probe. With evacuation and drying it disappears confirming its water-adsorption nature. It is to note as well that SBF 48 h apatite was synthesized via amorphous precursor, while the apatite displaying OH containing IR spectrum (Fig. 3b) was obtained via a low crystalline precursor prepared and transformed into more crystalline apatite using the same experimental protocol as for SBF 48 h sample.

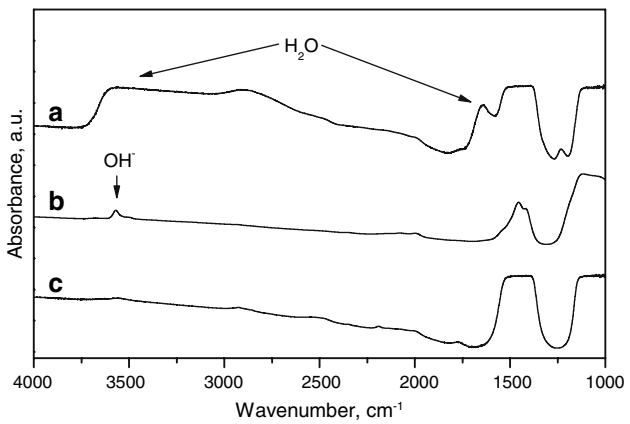

Fig. 3 Vacuum FTIR spectra of (**a**) SBF 48 h at room temperature, (**b**) a carbonate apatite after heating at 400 °C, and (**c**) SBF 48 h at 400 °C. Note that the lack of OH is not necessarily due to type A carbonate substitution but mainly to charge compensation mechanisms [32]

The elemental composition, the Ca/P molar ratio, and the specific surface areas of the samples are listed in Table 3. It should be noted that the elemental analysis of ACAP is not fully accurate due to the high water content which enables the occlusion of $CaCl_2$ and NaCl [3]. The carbonate content additionally increases the Ca/P molar ratio of ACAP. In accordance with the observations made by Kim et al. [4], ACAPs elevated Ca/P ratio decreases rapidly to about the theoretically expected value for ACP of 1.5 in the initial times of crystallisation after soaking in SBF due to dissolution of the occluded salts. Further, the Ca/P molar ratio increases and reaches the hydroxyapatite stoichiometric value of 1.67 [4]. The incorporation of the minor elements decreases with maturation but not necessarily with crystallinity, which suggests some calcium apatite self-cleaning ability. The specific surface area is strongly reduced from amorphous to crystalline state.

The SEM micrographs are shown in Fig. 4. The particles size ranges from about 20 nm to 60 nm and slightly increases with maturation due to Ostwald ripening [2]. Probably, the particles with smooth faces resembling crystal faces on Fig. 4c (marked with asterisk) are more crystalline than the particles without edges and clearly discernible faces (marked with arrow). If so, after 24 h soaking in SBF, an amorphous-like phase still exists, suggesting some stability of ACAP under the examined pseudo physiological conditions. The SBF solution is supersaturated with respect to calcium apatite [36] and therefore heterogeneous nucleation and subsequent crystal growth are to be expected (Fig. 4d). Notably, the SEM

Table 3 Elemental composition, Ca/P molar ratio, and specific surface area of the samples

Sample	Na (wt%)	Mg (wt%)	K (wt%)	Ca/P	SSA (m^2/g)
ACAP	2.36	0.15	0.099	1.95	285 ± 28[b]
SBF 2 h	0.96	0.68	0.097	1.51	–
SBF 24 h	0.38	0.57	0.004	1.64	190 ± 21
SBF 48 h	0.23	0.53	0.001	1.67	88 ± 9
Bone [1]	0.90[a]	0.72[a]	0.030[a]	1.5–1.7 [24]	100–200 [18]

[a] Data obtained with ashed specimens

[b] The specific surface area (SSA) of the samples is strongly influenced by the remaining water. Nevertheless, no heating was performed to avoid any crystallisation driven reduction of the SSA [35]. Therefore, the measured values are approximate and most likely underestimated

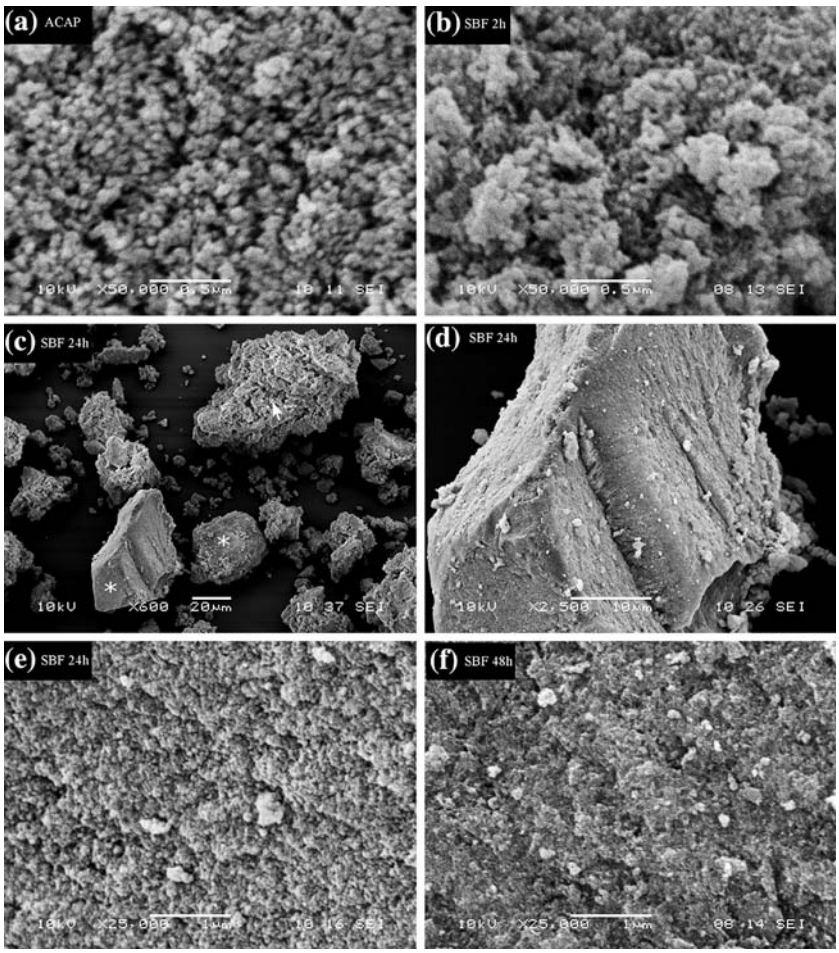

Fig. 4 SEM micrographs of (**a**) ACAP, (**b**) SBF 2 h, (**e**) SBF 24 h and (**f**) SBF 48 h showing the morphology of the samples, (**c**) SBF 24 h revealing the possible existence of both amorphous (white arrow) and crystalline (white asterisk) particles, and (**d**) SBF 24 h manifesting the secondary apatite crystallisation, i.e., the bright aggregates on the crystal face

images reveal some surface roughness and microporosity, due to the high water content generating voids with drying. This observation correlates well with the large surface area.

Discussion

Bone is constituted by organic and inorganic phases highly organised in several hierarchical levels [37]. Although most of the bone features are governed by the interactions between the protein matrix (mostly collagen), the calcium apatite mineral dispersed in it, and by the bone cells activities, functions attributed only to apatite are present.

The bone apatite is in the nanoscale with typical dimensions of 25–50 nm [1, 37]. The nanometer size provides at least two essential roles. The first one is related to the mechanical purpose of the hard tissues [38]. The second, due to thermodynamic reasons [39], is referred to the bone remodelling process where the matrix is degraded by the osteoclasts and reconstructed by the osteoblasts. Additionally, such a small crystal size is responsible for the large surface area of the bone apatite along with the surface roughness.

Bone apatite is low crystalline which increases solubility hence enhancing remodelling. Since calcium apatite is composed by Posner's clusters ($Ca_9(PO_4)_6$), it is suggested that the low crystallinity is mainly a result of the amorphous-to-crystalline transition where some clusters are not well stacked and/or stacking is incomplete [13], i.e., amorphous domains still exist. In addition carbonate content leads to structural mismatch [31, 40] thus decreasing crystallinity, which, in turn, increases solubility.

The importance of bone apatite as ion store is incontestable. Apart from calcium and phosphorus, minor amounts of magnesium, sodium and other elements are also available in case of necessity. The immune function should be mentioned as well since noxious elements such as Sr^{2+} or Pb^{2+} are incorporated to prevent intoxication. The large surface area (i.e., 100–200 m^2/g) makes some 20% of the bone accessible to body fluids [2], therefore favouring the element exchange and, if required, the fast bone remodelling, e.g., in case of fracture. At this point the question about the high content of carbonate (i.e., about 6 wt%) and the lack of OH groups arises. The osteoclasts resorb the inorganic part of bone by targeted secretion of HCl into the resorption lacuna resulting in local slightly acidic pH [41].

If there are any hydroxyl ions in the apatite, they will buffer the cell produced acid hence suppressing degradation [16]. On the other hand, a recent study reported the presence of hydroxyl groups in bone mineral at about 20% of the level observed in stoichiometric HAP [42]. Notably, in order to keep the mineral part of bone unaltered this investigation was made without any chemical pre-treatment. The question about hydroxyl content and its possible role in bone mineral remains to be clarified. Further, CO_2/HCO_3 is the main inorganic buffer of the human plasma [6]. Bone apatite is a source of carbonate ions thus actively participating in the maintaining of the physiological pH. The influence of carbonate content on the degree of crystallinity should also be emphasized as discussed above.

The supposed and unexpected stability of ACAP in simulated body fluid at 37 °C and the possible presence of amorphous phase even after 24 h of maturation are to be mentioned. Assuming an amorphous calcium phosphate (ACP) phase exists in bone, it is likely that the former has some physiologic role such as enhancing solubility [29, 43] and ensuring the mechanical isotropy, thus increasing the stiffness in all directions [44]. In fact, the amorphous calcium phosphate has comparable mechanical parameters to hydroxyapatite and β-tricalcium phosphate [29]. The real Ca/P ratio of the possible biogenic ACP is unknown but if this ratio is high, ACP could as well promote the calcium-mediated interactions between the mineralised collagen fibrils and the non-fibrous organic matrix, which holds the mineralised fibrils together [45].

The calcium apatite synthesized in this study possesses many of the known bone apatite features [1, 16, 18, 23, 24, 37]. It is known that A-type carbonate substitution can be obtained via high temperature and/or pressure synthesis [30–32]. Using amorphous precursor an A-type carbonate substitution is produced at a physiologic temperature and atmospheric pressure. The lack of OH is intriguing as well since it is impossible to control the incorporation of hydroxyl ions into the apatite lattice. Notably, only an amorphous precursor derived apatite is hydroxyl-free. Being low crystalline, the material exhibit nanometer size, specific surface area, and carbonate content in the same order as bone crystals. In addition, minor amounts magnesium and sodium, originating from the SBF, are present.

The existence of all these characteristics simultaneously in one material synthesized in vitro was much unexpected. It is likely that an amorphous-to-crystalline transition driven self-organisation takes place and causes the obtained bone resemblance.

Conclusion

In this study a biologically inspired strategy gives rise to bone-like apatite. Initially, a stable amorphous calcium apatite precursor was synthesized. The existence of the amorphous precursor and its biomimetic transformation into a crystalline phase seems to be the key event for the synthesis of a bone resembling calcium apatite.

Acknowledgements One of the authors (Ya. Pekounov) wishes to express his sincere gratitude to K. Chakarova for the IR technical assistance and to I. Dimov for his valuable help with the preparation of the manuscript.

References

1. S. V. DOROZHKIN and M. EPPLE, *Angew. Chem. Int. Ed.* **41** (1969) 3130
2. A. S. POSNER, *Physiol. Rev.* **49** (1969) 760
3. F. BETTS, N. C. BLUMENTHAL and A. S. POSNER, *J. Cryst. Growth* **53** (1981) 64
4. H. M. KIM, T. HIMENO, T. KOKUBO and T. NAKAMURA, *Biomaterials.* **26** (2005) 4366
5. A. C. TAS, *Biomaterials* **21** (2000) 1429
6. P. A. A. P. MARQUES, M. C. F. MAGALHÃES and R. N. CORREIA, *Biomaterials.* **24** (2003) 1541
7. A. BIGI, E. BOANINI, S. PANZAVOLTA and N. ROVERI, *Biomacromolecules.* **1** (2000) 752
8. A. BIGI, E. BOANINI, S. PANZAVOLTA, N. ROVERI and K. RUBINI, *J. Biomed. Mater. Res.* **59** (2002) 709
9. K. ONUMA, *J. Phys. Chem. B.* **109** (2005) 8257
10. G. HE, T. DAHL, A. VEIS and A. GEORGE, *Nat. Mater.* **2** (2003) 552
11. W. B. VALHMU, L. N. Y. WU and R. E. WUTHIER, *Bone Miner.* **8** (1990) 195
12. L. N. Y. WU, G. R. SAUER, B. R. GENGE, W. B. VALHMU and R. E. WUTHIER, *J. Inorg. Biochem.* **94** (2003) 221
13. K. ONUMA and A. ITO, *Chem. Mater.* **10** (1998) 3346
14. A. OYANE, K. ONUMA, A. ITO, H. M. KIM, T. KOKUBO and T. NAKAMURA, *J. Biomed. Mater. Res.* **64A** (2003) 339
15. X. YIN and M. J. STOTT, *J. Chem. Phys.* **118** (2003) 3717
16. J. D. PASTERIS, B. WOPENKA, J. J. FREEMAN, K. ROGERS, E. VALSAMI-JONES, J. A. M. VAN DER HOUWEN and M. J. SILVA, *Biomaterials.* **25** (2004) 229
17. C. REY, J. L. MIQUEL, L. FACCHINI, A. P. LEGRAND and M. J. GLIMCHER, *Bone* **16** (1995) 583
18. A. S. POSNER, *J. Biomed. Mater. Res.* **19** (1985) 241
19. K. KANDORI, S. SAWAI, Y. YAMAMOTO, H. SAITO and T. ISHIKAWA, *Colloid Surf.* **68** (1992) 283
20. A. L. BOSKEY and A. S. POSNER, *J. Phys. Chem.* **77** (1973) 2313
21. F. ABBONA, H. E. L. MADSEN and R. BOISTELLE, *J. Cryst. Growth* **74** (1986) 581
22. S. KRUMM, *Mat. Sci. Forum* **228–231** (1999) 183
23. F. PETERS, K. SCHWARZ and M. EPPLE, *Thermochim. Acta* **361** (2000) 131
24. A. BIGI, G. COJAZZI, S. PANZAVOLTA, A. RIPAMONTI, N. ROVERI, M. ROMANELLO, K. NORIS Suarez and L. MORO, *J. Inorg. Biochem.* **68** (1997) 45
25. G. M. BLIZNAKOV, I. V. BAKARDJIEV and E. M. GOCHEVA, *J. Catal.* **18** (1970) 260
26. S. UOIZAT, A. BARROUG, A. LEGROURI and C. REY, *Mater. Res. Bull.* **34** (1999) 2279
27. M. G. TAYLOR, S. F. PARKER, K. SIMKISS and P. C. H. MITCHELL, *Phys. Chem. Chem. Phys.* **3** (2001) 1514
28. N. C. BLUMENTHAL, A. S. POSNER and J. M. HOLMES, *Mater. Res. Bull.* **7** (1972) 1181

29. D. TADIC, F. PETERS and M. EPPLE, *Biomaterials* **23** (2002) 2553
30. M. E. FLEET, X. LIU and P. L. KING, *Am. Miner.* **89** (2004) 1422
31. M. E. FLEET and X. LIU, *J. Solid State Chem.* **177** (2004) 3174
32. R. ASTALA and M. J. STOTT, *Chem. Mater.* **17** (2005) 4125
33. S. KOUTSOPOULOS, *J. Biomed. Mater. Res.* **62** (2002) 600
34. G. BUSCA, V. LORENZELLI, P. GALLI, A. LA GINESTRA and P. PATRONO, *J. Chem. Soc., Faraday Trans.* **183** (1987) 853
35. K. D. ROGERS, P. DANIELS, *Biomaterials* **23** (2002) 2577
36. L. XIONG and Y. LENG, *Biomaterials* **26** (2005) 1097
37. S. WEINER and H. D. WAGNER, *Annu. Rev. Mater. Sci.* **28** (1998) 271
38. H. GAO, B. JI, I. L. JÄGER, E. ARZT and P. FRATZL, *Proc. Natl. Acad. Sci. USA* **100** (2003) 5597
39. R. TANG, L. WANG, C. A. ORME, T. BONSTEIN, P. J. BUSH and G. H. NANCOLLAS, *Angew. Chem. Int. Ed.* **43** (2004) 2697
40. A. A. BAIG, J. L. FOX, R. A. YOUNG, Z. WANG, J. HSU, W. I. HIGUCHI, A. CHETTRY, H. ZHUANG and M. OTSUKA, *Calcif. Tissue. Int.* **64** (1999) 437
41. H. K. VÄÄNÄNEN, H. ZHAO, M. MULARI and J. M. HALLEEN, *J. Cell. Sci.* **113** (2000) 377
42. G. CHO, Y. WU and J. L. ACKERMAN, *Science* **300** (2003) 1123
43. M. R. SARKAR, N. WACHTER, P. PATKA and L. KINZL, *J. Biomed. Mater. Res.* **58** (2001) 329
44. L. ADDADI, S. RAZ and S. WEINER, *Adv. Mater.* **15** (2003) 959
45. G. E. FANTNER, T. HASSENKAM, J. H. KINDT, J. C. WEAVER, H. BIRKEDAL, L. PECHENIK, J. A. CUTRONI, G. A. G. CIDADE, G. D. STUCKY, D. E. MORSE and P. K. HANSMA, *Nat. Mater.* **4** (2005) 612